JOURNAL OF OPTOELECTRONICS AND ADVANCED MATERIALS, Vol. 11, No. 1, January 2008, p. 45 - 55

# Magnetostrictive behaviour of ribbons and wires: analytical modelling and experimental validation

A. MAMALIS, E. HRISTOFOROU*
*National Technical University of Athens, Zografou Campus, Athens 15780, Greece*

In this paper the magnetostrictive behaviour of ribbons and wires is revisited and studied, proposing an analytical modelling followed by experimental validation using the magnetostrictive delay line (MDL) method, due to the needs for engineering applications of magnetostriction, like sensors and transducers. The obtained results may be used for the determination of the M(H) and λ(H) functions as well as their uniformity distribution along the length of magnetostrictive ribbons and wires, which is a key-factor for the characteristics of sensors based on the magnetostriction effect.

(Received November 24, 2008; accepted January 21, 2009)

*Keywords*: Magnetostriction, Analytical modeling, Ribbons, Wires, Sensors

## 1. Introduction

Sensors and transducers have an increasing interest because of their importance in many technological applications [1]. All modern vehicles and transportation means use a vast variety of sensors and transducers, thus allowing a safer and more comfortable way of driving and commuting. The operation of all medical instruments is based on sensors. Industry is also employing more and more transducers for the monitoring and control of production lines. In the literature, sensors have been categorized in several ways [2]. In the present work, they are categorized according to the following three principles: the first one is the subject of measurement, the most significant divisions being physical and chemical sensors; the second principle concerns the physical phenomenon and material on which the operation of the sensor is based, the main categories being conducting, semiconducting, dielectric, magnetic and superconducting sensors; and the third one concerns their applications, the main categories being industrial, transportation, automotive, medical, military, domestic and environmental sensors.

Magnetic sensors play a significant role in physical measurements used in all kinds of applications [3, 4]. The most often used magnetic phenomena in today's magnetic sensor technology are the magneto-resistance [5], the magneto-impedance [6], the magnetostriction [7], the electromagnetic induction [8] and the Hall effect [9]. The dynamics of magnetic domains is the main mechanism responsible for magnetic effects used in sensing applications [10]. Any possible use of the dynamic response of this mechanism can result in a sensing element. There are two distinct cases of domain dynamics, one of which is the domain wall dynamics and the other one the domain rotation dynamics. There also exist dependent effects derived from these dynamics, both macroscopic and microscopic.

Magnetostriction, a particular effect in magnetic materials, has been thoroughly investigated in terms of theory and modeling as well as in terms of experimental details and applications [11-15]. The theory of magnetostriction is mainly based on the principles of micromagnetics [16]. The applications concern sensors and actuators, requiring materials of engineering magnetostriction constant in the order of 10 ppm and 1000 ppm, respectively.

A technique that utilizes the magnetostriction effect in the design and development of sensors measuring displacement, stress and field is the magnetostrictive delay line (MDL) technique [17]. In this work, the magnetostrictive behavior of ribbons and wires able to operate as MDLs is analytically modeled, followed by experimental validation. The presented model may be used for the determination of the M(H) and λ(H) loops as well as their non non-uniformity distribution along their length.

## 2. Magnetization effects contributing to magnetostriction

The main magnetization effects contributing to magnetostriction are based on domain wall and domain rotation dynamics as well as the macroscopic and microscopic mechanisms dependent on domain dynamics. These effects are briefly presented bearing in mind that a key parameter in the magnetostrictive behavior is the hysteresis in their response. Hysteresis should be negligible in applications like mechanical and field sensors in order to improve the uncertainty level of the sensors, but it should be heavily present in applications like security sensors to improve the stability of the stored information.

### *2.1. Domain wall dynamics.*

The dynamics of domain walls and their corresponding use in sensor applications concern their nucleation and mobility or propagation in the magnetic substance [18]. There are two mechanisms of domain wall propagation, namely the bowing process and the parallel motion of the domain walls. The mode of propagation depends on the energy stored in these walls. Low energy walls propagate through the bowing process as shown in Fig. 1a while high energy walls propagate more rigidly as shown in Figure 1b. The bowing process is more likely to occur in soft magnetic materials, which are low pinning materials, while the more rigid motion occurs in the harder ones. The reversibility of the domain wall propagation determines the presence or not of hysteresis in the phenomenon used in the sensing element and depends mainly on the defects in the magnetic substance and the pinning effect of magnetic dipoles. Domain wall dynamics are used for small field measurements as well as for mechanical sensors based on small field measurements [19].

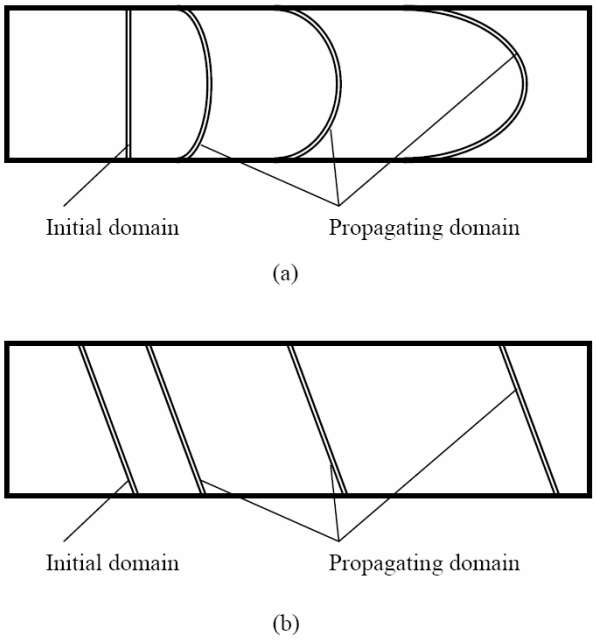


*Fig. 1. Modes of propagation of domain walls. (a) Low energy walls (b) high energy walls*

Therefore, the sensor designer using domain wall dynamics should tailor the magnetic material with respect to the application in request. If the case is a sensor based on domain wall propagation with hysteresis in the minimum possible amplitude, the material should include as less defects as possible and be as soft as possible. This may be controlled through the composition of the material, as well as through annealing of the material in order to minimize the internal stresses generated by the above-mentioned defects, targeting coercive fields of the order of 1 A/m [20]. In this case, the material should have low magnetostriction and correspondingly low magneto-elastic response to avoid cross-talk with possibly uncontrollable stray magneto-elastic waves. One can fulfil both requirements by using FeCoSiB wires of magnetostriction in levels of 0.1 ppm, after thermal annealing and sometimes magnetic field annealing [21], while using a magnetostrictive substance may result in high levels of Barkhausen noise. Typical annealing conditions are of the order of 30-60 $^{o}$C/min for the rising temperature, steady state conditions of 300$^{o}$C – 750 $^{o}$C for 10 – 60 minutes and finally slow cooling in Ar atmosphere for about 12-24 hours. Typical field conditions during annealing are 800 – 8000 A/m. Another technique also used in the material tailoring is the stress – current annealing, with typical values of tensile stress and current of 100 – 500 MPa and 100 – 300 mA respectively [22]. On the contrary, in security sensors the pinning defects or the controllable introduction of defects on the surface of the material can result in a significant improvement of the sensor stability.

### *2.2. Domain rotation dynamics.*

Domain rotation dynamics have two distinct areas of operation, the irreversible and the reversible area [23]. Irreversible rotation occurs when the magnetic domains, oriented along a given easy axis A, re-orient along another easy axis B, closer to the axis of the external field H, because of the presence of this field, as shown in Figure2a. Reversible domain rotation occurs after the irreversible rotation process has taken place. Since the new easy axis B is, in general, not the same as the axis of the external field H, the magnetic dipoles rotate reversibly towards the axis of the external field H, as shown in Fig. 2b. After the removal of the external field, the magnetic domains rotate back to the easy axis direction B, along which they had been initially and irreversibly re-orientated. In general, magnetic domains do not return back to their initial easy axis A. Both reversible and irreversible processes are associated with the presence of magnetostriction. The irreversible process is additionally responsible for the small or large Barkhausen jumps, introducing magnetic noise in the sensing element. Employing the irreversible process results in hysteresis in magnetic rotation, as well as in a relatively higher level of noise with respect to the reversible process. Both hysteresis and noise affect the uncertainty of any possible magnetic device used for sensing. Therefore, if the aim is the development of a sensor, where hysteresis and noise should be minimized, only the reversible area of domain rotation should be used. On the contrary if the aim is high hysteresis, the irreversible area of the domain rotation should be used. The domain rotation effect has found applications mainly in the field of mechanical sensors [24]. The dynamic behaviour of these processes can result in elastic waves, propagating along the magnetic substance. This is precisely the basis of the MDL technique [25-28]. The MDL technique has been extensively studied in order to understand its operation and optimize its performance [29-32] using a variety of methods [33-37].

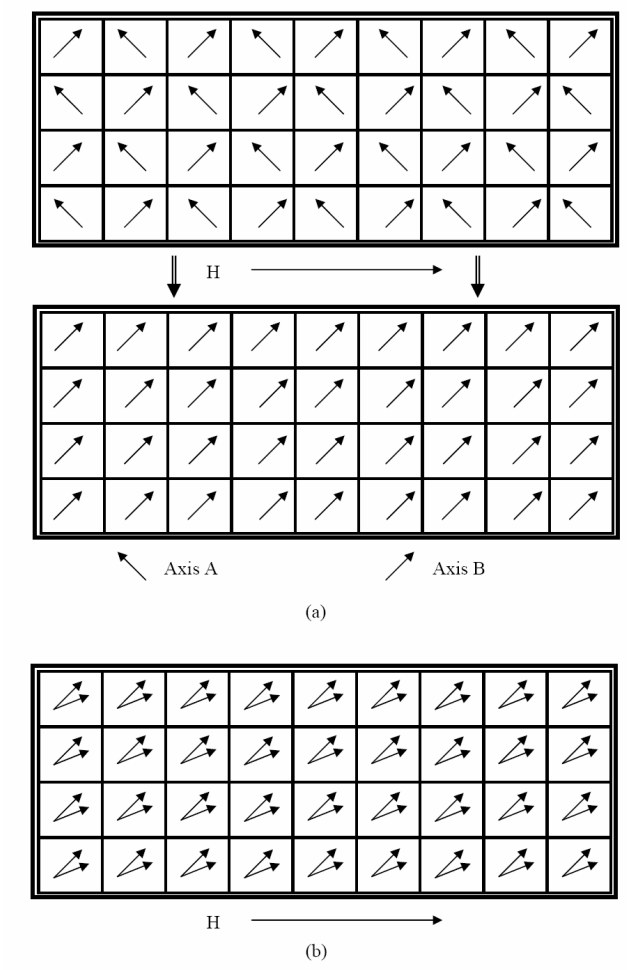


*Fig. 2. Irreversible and reversible rotation in magnetic domains. (a) Irreversible orientation along easy axis A or B, (b) Reversible small magnetization angle rotation (SMAR)*

A vast variety of magnetostrictive materials have been developed up to now. Today, the materials exhibiting the largest possible magnetostriction are the recently developed magnetic shape memory (MSM) alloys [38], exhibiting dimensional changes in the order of 1% to 10%. Their operation is based on the martensitic – austenitic transformation even at room temperature due to the change of the biasing field.

Before the development of MSM alloys, the materials exhibiting the largest magnetostriction were the rare earth – transition metal alloys, with saturation magnetostriction in the order of 800 ppm to 2000 ppm [39-41]. Combination of rare earth elements and magnetic substances, like iron, nickel and cobalt, resulted in the development of Terfenol and other similar alloys, which have been extensively used in engineering applications.

Soft magnetostrictive alloys based on iron, nickel and cobalt exhibit a relatively low magnetostriction in the order of 30-100 ppm and are generally used as MDLs. The needs in modern sensor development would not allow for the use of the classical polycrystalline materials and led to the development of the amorphous magnetostrictive alloys, like ribbons, wires and glass-covered wires, prepared by rapid quenching techniques [42-46].

The amorphicity of the used magnetostrictive material helps in the minimization of the irreversible rotation process, because of the minimization of the coercive field and the field range responsible for the irreversible domain rotation. The need for miniaturization has led research groups to develop MDL arrangements in thin film structure, thus enhancing the possibility of developing integrated systems [47-49]. Furthermore, the need for better sensor characteristics has led to the development of nano-crystalline magnetostrictive ribbons and wires [50, 51] with even lower hysteresis, which can be used as MDLs, provided that they can exhibit magnetostriction. Recently, an interesting composite material including magnetostrictive substance in a non-magnetic matrix has been proposed for magnetoelastic applications [52].

When designing a sensor using the effect of domain rotation, one should tailor the magnetic material in order to minimize the amplitude of the external field responsible for the irreversible rotation process and correspondingly maximize the external field range for reversible rotation. Annealing techniques have been employed, targeting the proper tailoring of the magnetostrictive elements [53-55]. These techniques mainly include heat annealing, field annealing and stress-current annealing, not only eliminating the defects of the material, but also re-orienting the magnetic anisotropy in order to eliminate the irreversible swift process of the domain rotation. The elimination of the irreversible process occurs simply because of the absence of an easy axis direction near the direction of the external field H. In this case, the magnetic field in the field annealing process should be perpendicular to the easy axis of the material. The magnitudes of temperature and field are similar to those in the case of domain wall dynamics.

The $\lambda(H)$ function is the most important characteristic regarding the MDL operation, since it can model the operation of an MDL set-up and consequently a sensor arrangement based on the MDL technique. Proper tailoring should take into consideration the dynamic response of $\lambda(H)$ with respect to frequency and not only the saturation magnetostriction constant $\lambda_s$ or the static magnetostriction function. A number of instruments have been developed in order to measure the dynamic characteristics of this function as well as the engineering magnetostriction constant $\lambda_s$ [56-58]. An excellent review of such measurement techniques is given in [59].

### *2.3. Dependent mechanisms.*

Apart from the domain wall and domain rotation dynamics, there are other dependent magnetic effects, which can be measured and used as macroscopic electrical and magnetic properties of the material.

The most well-known and used effect is the magneto-resistance effect [60], observed mainly in magnetic thin films. According to this effect, the dc electrical resistance of a magnetic film changes about 2-3%, with respect to the externally applied magnetic field, due to the magnetic

domain rotation and in some cases due to domain wall nucleation. The most significant magneto-resistive effect, the "giant" magneto-resistive effect, appears in magnetic thin film multi-layers where the change in resistance hovers in the range of 50-80% at room temperature. This "giant" effect is due to the perpendicular anisotropy of the magnetic layers causing a large magnetic moment rotation. Recently, the "colossal" magneto-resistive effect has been observed in magnetic oxides, offering even larger changes in resistance, but in cryogenic environments. The magneto-resistive effect is mainly used in field sensors and recording media applications. Another effect, which has also found applications, is the ac magneto-resistance effect or magneto-impedance effect [61-63]. According to this effect, the ac resistance or impedance of a magnetic substance varies with the applied field. This effect also exists in non-ferromagnetic materials due to the skin effect, although its amplitude is much smaller than in ferromagnetic materials.

In some zero-magnetostrictive wires, with circumferential magnetic anisotropy, the magneto-impedance changes more than 100% with respect to the applied external field. Although this effect has only recently been studied, it has already been used in industrial and automotive applications due to its great sensitivity in magnetic field.

Recently, another effect attracts the interest of the field sensor market and mainly the recording media market. This is the spin valve effect [64-66], according to which an especially designed magnetic arrangement exhibits non-symmetrical B-H response. This property allows very well localized field measurements with an acceptable accuracy. Apart from that, the spin tunneling effect has also been used in recording media and accurate field measurements [67].

Apart from these, the rather classical inductive effects [68] have been implemented in the form of the fluxgate set-up [69] for accurate field detection and linear variable differential transformer (LVDT) for displacement sensing [70]. Other related electromagnetic effects such as the Hall effect, the Quantum Hall effect and the SQUID are also able to detect field. With the exception of magneto-elasticity, which is used for direct detection of mechanical sizes, the main sensing application of magnetic effects and materials is the detection of magnetic field. Once the field or field change has been measured, one can map the measurement to another physical size, like displacement, stress, flow etc.

## 3. Analytical modeling of the basic MDL arrangement

The most classical MDL arrangement, the coil-coil MDL set-up, is shown in Fig. 3. A short excitation coil and a short search (named also detecting or receiving) coil are placed around each one of the two ends of the MDL. The delay line is terminated using latex adhesive to eliminate acoustic reflections. Details of the various versions of such arrangements can be found in [71, 72] and are presented hereinafter.

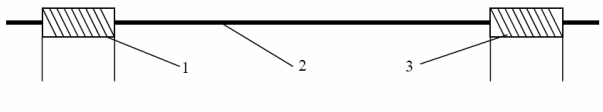


*Fig. 3. The basic MDL arrangement. (1) Excitation coil, (2) Magnetostrictive delay line, (3) Search coil.*

Magnetostrictive materials subjected to either low or high frequency fields, tend to undergo either domain wall motion or magnetic domain rotation respectively, always towards the direction of the externally applied field. Thus, applying external bias or pulsed field along the MDL axis results initially in Barkhausen jumps, which contribute to the hysteretic and irreversible part of the $\lambda(H)$ function and consequently in small angle rotation which is the anhysteretic and reversible part of the said $\lambda(H)$ function.

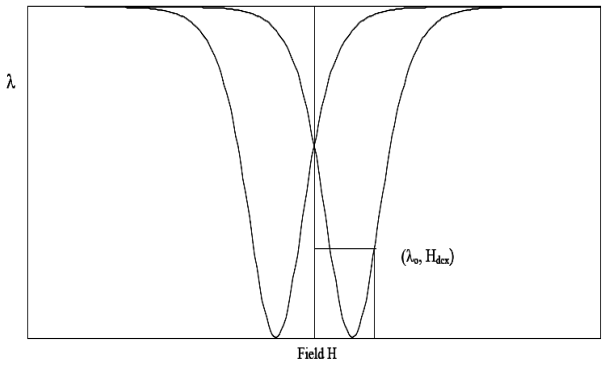


*Fig. 4. A typical λ(H) function.*

Therefore, polarizing the MDL with a dc bias field $H_{dcx}$, results in an elongation of the material $\delta\lambda_o$, illustrated as a point $(\delta\lambda_o, H_{dcx})$ on the $\lambda(H)$ function, shown on Fig. 4. When a pulsed field $H_e(t)$ is additionally applied at the region where the bias field has been applied, a similar but dynamic elongation $\delta\lambda(t)$ occurs, as shown in Fig. 5, resulting in an elastic wave propagating along the MDL, following the classical wave equation, as shown in Fig. 6.

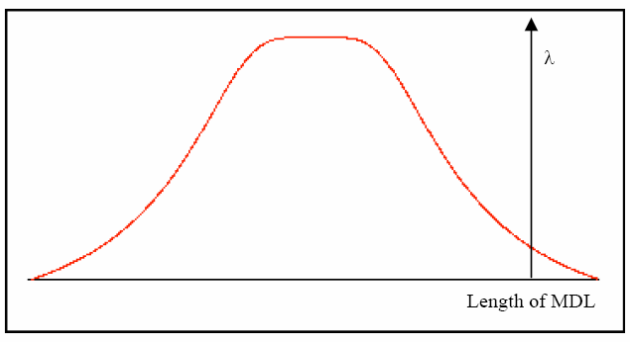


*Fig. 5. Microstrain with respect to space.*

In classical magnetostrictive materials, the optimum pulsed field width is in the order of μs. Thus, the wavelength of the propagating elastic wave is in the order of several mm. Therefore, in the most common MDL elements, where the MDL cross section is a tenth of $mm^2$, a Lamb wave is propagating. Using materials with higher frequency response or larger cross section can result in surface acoustic wave propagation. Skin effect plays an important role in modeling and tailoring the behaviour of the microstrain generation and propagation.

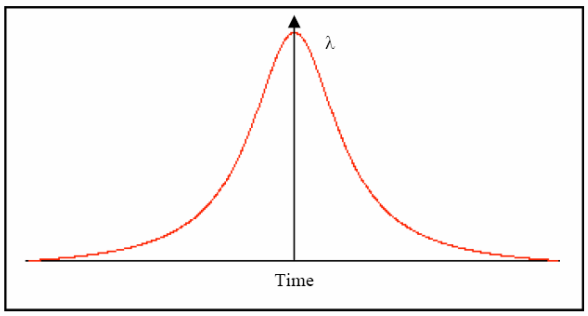


*Fig. 6. Propagating elastic pulse along the length of the MDL.*

The pulsed field along the MDL, responsible for the elastic wave generation follows a decaying profile extending from the fully magnetized central region to a limit which is practically of the order of the excitation coil diameter, indicating the active region of the magnetostrictive material involved in the microstrain generation.

This elastic wave propagates along the length of the MDL, mainly as a longitudinal elastic wave, because of the shape of the acoustic wave guide: the short cross section with respect to the wavelength and the dimensions of the MDL eliminate any transverse and quasi-transverse waves.

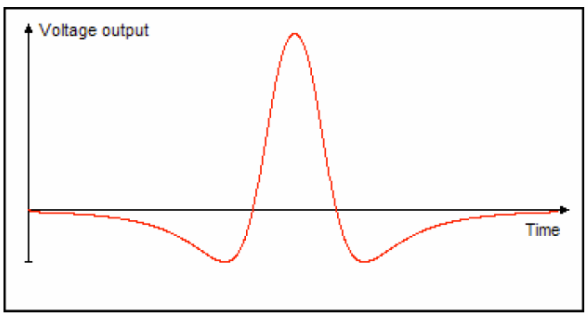


*Fig. 7. Voltage output with respect to time.*

The propagating elastic wave, in its course, changes the local magnetization component along the MDL axis, provided that the MDL is locally magnetized. The total, macroscopic change of the magnetic flux along the axis of the wire is the result of the statistical sum of local infinitesimal changes in the orientation of magnetic dipoles, in the course of the propagating elastic wave. Thus, the magnitude of the biasing field determines the change of the local magnetization component along the MDL axis. This is actually the inverse magnetostriction effect. In some materials, the earth's field can be enough to polarize and consequently cause the presence of such effect.

Thus, if an inductive means, like a search coil, is set around the MDL, a pulsed voltage proportional to the first derivative of the flux is induced across its ends, as shown in Fig. 7. The search coil should be set at a distance x from the elastic wave point of origin (PO), which ought to be small enough to cause negligible attenuation and large enough to avoid electromagnetic coupling between excitation and detection means. Such pulsed voltage output is received with a delay time proportional to the distance x and inversely proportional to the longitudinal sound velocity of the magnetostrictive element. A real pulsed voltage output waveform, with the corresponding delay time from the excitation pulse observed as impulse response, is shown in Fig. 8. In this case, the relatively small waveforms following the main pulse are due to reflections of the propagating elastic pulse.

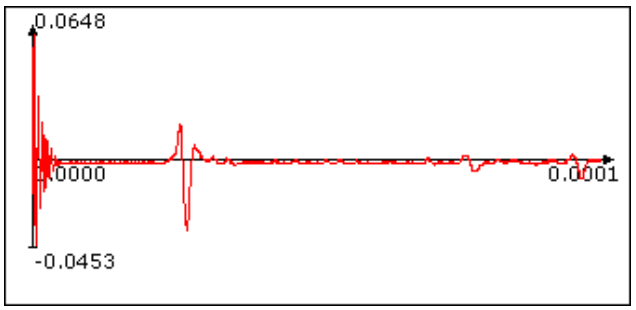


*Fig. 8. The detected MDL pulsed voltage output. The first impulse response is due to the pulsed excitation field. The main pulsed voltage output follows, with a characteristic amplitude $V_o$. The small waveforms following the main pulsed output are reflections of the propagating elastic pulse at the ends of the magnetostrictive medium (Time units in seconds and voltage amplitude in Volts).*

### *3.1. Magnetostriction modeling*

At the atomic level, magnetostriction is the aggregate result of the deformations of the crystal lattices inside the domains that tend to align with the domain magnetization. The deformation of a crystal lattice is due to the interactions between the atomic moments occupying its sites that result in altering the bond lengths. When the bonds lie at an angle $\phi$ to the domain magnetization, the magnetoelastic energy tends to align the bonds with the domain magnetization, but is counterbalanced by the elastic bond energy. At the macroscopic level, one can think of the energy added to the system because of an

externally applied field, $\Delta E_m$, as being counterbalanced by the change in elastic bond energy, $\Delta E_{el}$ along the MDL axis:

$$\Delta E_m = \Delta E_{el} \Leftrightarrow \Delta M \cdot \Delta H = \frac{1}{2} k \Delta\lambda^2 \Leftrightarrow \frac{\Delta M}{\Delta H} = \frac{1}{2} k \left( \frac{\Delta\lambda}{\Delta H} \right)^2 \tag{1}$$

where k is the macroscopic elastic constant of the material, related to Young's modulus $E_Y$, and $\Delta\lambda$ is the elongation caused by the change in magnetization ΔM.

$$\text{For } \Delta H \to 0, \frac{d\lambda}{dH} \propto \sqrt{\frac{dM}{dH}}$$

The derivative $\frac{dM}{dH}$ corresponds to the differential susceptibility $\chi_{diff}$, of the magnetic material, which can be described by a function of the form:

$$\chi_{diff} = \frac{dM}{dH} \propto \left( \frac{H}{c} + \chi_0 \right) e^{-\frac{H}{c}} \tag{2}$$

where $c$ is a fitting constant with field dimensions related to $K_1$ and $M_s$ [73] and $\chi_0$ the initial susceptibility. The above mentioned equation is the solution to a second order linear differential equation whose characteristic equation is: $x^2 + cx + c = 0$, as in the critical damping case in resonance. Thus

$$\frac{d\lambda}{dH} \propto \lambda_s \sqrt{\left( \frac{|H|}{c} + \chi_0 \right) e^{-\frac{|H|}{c}}} = \lambda_s e^{\frac{\chi_0}{2}} \sqrt{\frac{|H|}{c} + \chi_0} e^{-\frac{1}{2}\left( \frac{|H|}{c} + \chi_0 \right)} \tag{3}$$

where $\lambda_s$ the saturation magnetostriction constant. Hence:

$$\lambda(H) = \int \frac{d\lambda}{dH} \propto \lambda_s e^{\frac{\chi_0}{2}} \int \sqrt{\frac{|H|}{c} + \chi_0} \cdot e^{-\frac{1}{2}\left( \frac{|H|}{c} + \chi_0 \right)} dH =$$

$$= \lambda_s e^{\frac{\chi_0}{2}} \left( \frac{\sqrt{u} \cdot erf\left( \sqrt{\frac{1}{2}\left( \frac{|H|}{c} + \chi_0 \right)} \right)}{4\sqrt{2}} - 2e^{-\frac{1}{2}\left( \frac{|H|}{c} + \chi_0 \right)} \cdot \sqrt{\left( \frac{|H|}{c} + \chi_0 \right)} \right) \tag{4}$$

where $erf(x)$ is the error function and:

$$erf\left( \sqrt{\frac{1}{2}\left( \frac{|H|}{c} + \chi_0 \right)} \right) = \frac{2}{\sqrt{\pi}} \int_0^x e^{\left( \frac{|H|}{c} + \chi_0 \right)} dx = \frac{2}{\sqrt{\pi}} \sum_{n=0}^{\infty} \frac{(-1)^n}{n!(2n+1)} x^{2n+1} \tag{5}$$

Thus:

$$\lambda(H) \propto \lambda_s e^{\frac{\chi_0}{2}} \left( \frac{\sqrt{u} \cdot \sum_{n=0}^{\infty} \frac{(-1)^n}{n!(2n+1)} x^{2n+1}}{2\sqrt{2\pi}} - 2e^{-\frac{1}{2}\left( \frac{|H|}{c} + \chi_0 \right)} \cdot \sqrt{\frac{|H|}{c} + \chi_0} \right), x = \frac{1}{2}\left( \frac{|H|}{c} + \chi_0 \right) \tag{6}$$

Experimental data, have illustrated that in the case of anhysteretic behaviour, the $\lambda(H)$ function can be fitted by $\lambda(H) = \lambda_s \left( 1 - e^{-cH^2} \right), c > 0$, where the positive number $c$ is an adaptive parameter. In the case of hysteretic evidence this model could become $\lambda(H) = \lambda_s \left( 1 - e^{-c(H \pm H_c)^2} \right), c > 0$.

The Energetic Model (EM) described in [74] relates the fitting constant $c$ to microscopic parameters of the material. At weak fields,

$$c = \left( \frac{M_s}{\chi_0} \right)^2 = \left( \frac{q \cdot k}{\mu_0 \cdot M_s} \right)^2 = \left( \frac{c_q \cdot K_1}{\mu_0 \cdot M_s} \right)^2 \tag{7}$$

and at strong fields,

$$c = \frac{2g \cdot H_s^{\,2}}{g + \sqrt{2 - 4g + g^2}} \approx H_s^{\,2} = \left( \frac{c_g' \cdot K_1}{\mu_0 \cdot M_s} \right)^2 \tag{8}$$

where g, h, k, q are the parameters of the EM:

$$g = \left( c_g \cdot \frac{\mu \cdot M_s^{\,2}}{K_1} \right), \; h = \frac{H_s}{\exp(g \cdot \ln 2)},$$

$$k = c_k \cdot E_Y \cdot \lambda_s^{\,2}, \; q = \frac{c_q}{c_k} \cdot \frac{K_1}{E_Y \cdot \lambda_s^{\,2}} \tag{9}$$

with $c_g$, $c_h$, $c_k$ and $c_q$ being the model's dimensionless microscopic constants. With the anisotropy field $H_k = \frac{2K_1}{\mu_0 \cdot M_s}$, the saturation field $H_s = \frac{c_g' \cdot H_k}{2}$ ($c_g'$ is a proportionality constant) and $c_q$ and $c_g'$ being of the same order of magnitude, an average value for $c$ at both weak and strong fields is defined by

$$c = 2\frac{c_q \cdot c_g'}{c_q + c_g'} \cdot \left( \frac{K_1}{\mu_0 \cdot M_s} \right)^2 = \left( \frac{H_s}{c'} \right)^2$$

In order to prove the principle of the described formalism, experimental data were obtained using a $Fe_{78}Si_7B_{15}$ amorphous ribbon MDL, exhibiting $\lambda_s$~30-32 ppm. The sample was previously stress-current annealed under 350 MPa and 100 mA, to remove internal stresses and improve its magnetostrictive behavior and uniformity of magnetic domains. The MDL set-up was operating by

incrementing the peak value of the pulsed current $I_e$ from 1 to 13.6A and back. The bias field at the arrangement was varied from 0 to 130 A/m at each $I_e$ amplitude. The output voltage is related to the dynamic response of the anhysteretic λ(H) function and is a function of the pulsed current waveform.

The peak voltage is maximum at a bias field of 16 A/m for all $I_e$. Considering the induced voltage,

$$V(t) \propto \frac{dB}{dt} \propto H_{dc}\frac{d\lambda}{dt} = H_{dc}\frac{d\lambda}{dH_e}\frac{dH_e}{dt} \Rightarrow V_0 = H_{dc}\max\left\{\frac{dH_e}{dt}\right\}\frac{d\lambda}{dH_e} = A_0\frac{d\lambda}{dH_e} \tag{9}$$

where $A_0$ is a constant related to $I_e$ and $\lambda_s$.

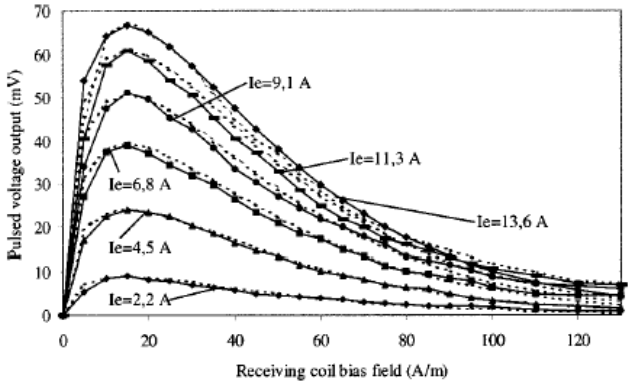


*Fig. 9. Comparison of experimental and theoretical data for biasing field using equation 1.1 to 1.5.*

Fig. 9 shows the experimental and theoretical data, concerning the dependence of the MDL peak amplitude $V_o$ on the DC bias field at the region of the receiving coil, at various values of $I_e$, producing the field $H_e$, for several amplitudes of $I_e$. As expected, the value of c turns out to be the same for all theoretical curves: c=15 A/m. This suggests that c is indeed related to material constants. $A_0$ exhibits a linear dependence on $I_e$ with signs of saturation for higher currents.

### *3.2. An alternative way of modeling the coil-coil MDL arrangement*

Following the basic MDL set-up as illustrated in Fig. 3, the MDL is activated by transmitting pulsed current $H_e(t) = H_e \cdot f(t)$, through the excitation coil or the pulsed current conductor. Pulsed current generates a pulsed magnetic field along the magnetostrictive element. This field generates a pulsed microstrain at the region of excitation of the magnetostrictive element, $\lambda(H_{oe} + H_e(t))$ due to the magnetostriction effect. Since the magnetostrictive material is in the shape of cylinder or ribbon, it can operate as acoustic waveguide. Therefore, the pulsed microstrain propagates along the length of the magnetostrictive element as longitudinal acoustic pulse. As soon as it arrives at the region of the search coil, it is detected as pulsed voltage output, proportional to the first derivative of the propagating pulse, due to the inverse magnetostriction effect. The generation and detection of the pulsed microstrain is possible and repeatable due to the presence of biasing fields at the acoustic stress point of origin and the search area, $H_{oe}$ and $H_{or}$ respectively, which orient the magnetic dipoles in a given direction.

The propagating pulsed microstrain induces stresses $\sigma(\lambda)$ in the MDL. These stresses act as effective field $H_\sigma = f(\sigma)$ in the MDL, added in the already existing biasing field along its length. Provided that the microstrain propagates without dispersion and after effects, which is applicable for the front acoustic wave, it arrives at the region of the search coil, inducing such an effective field $H_\sigma$ along the length of the MDL. Thus, the flux within the magnetic region inside the search coil is:

$$\Phi(t) = S \cdot \mu(H_{or}) \cdot (H_{or} + H_\sigma) \tag{10}$$

where $S$ is the cross section of the magnetostrictive element. Thus, the voltage output $V_o(t)$ at the search coil is:

$$V_o(t) = -\frac{d\Phi}{dt} = -A \cdot \mu(H_{or}) \cdot \frac{dH_\sigma}{dt} \tag{11}$$

Where $A$ includes $S$ and search coil parameters. Provided that excitation pulsed field is relatively small, the effective field and stress are assumed to be proportionally related:

$$H_\sigma = f(\sigma) = a \cdot \lambda(H_{oe} + H_e(t)) \tag{12}$$

Thus $V_o(t)$ becomes:

$$V_o(t) = -A \cdot a \cdot \mu(H_{or}) \cdot \frac{d\lambda(H_{oe} + H_e(t))}{dt} = -A \cdot a \cdot \mu(H_{or}) \cdot \frac{d\lambda}{dH}\frac{d(H_{oe} + H_e(t))}{dt}$$
$$= -A \cdot a \cdot \mu(H_{or}) \cdot \frac{d\lambda}{dH} \cdot H_e \cdot \frac{df(t)}{dt} \tag{13}$$

Thus the peak to peak magnitude of $V_o(t)$, $V_o$ is given by:

$$V_o = -A \cdot a \cdot c \cdot H_e \cdot \mu(H_{or}) \cdot \frac{d\lambda}{dH} \tag{14}$$

where $c$ is the maximum of $\frac{df(t)}{dt}$.

In the case that $H_e, H_{oe}$ are not changing and $H_{or}$ changes, $V_o$ becomes:

$$V_o = -A \cdot a \cdot c \cdot c_1 \cdot H_e \cdot \mu(H_{or}) = C_1 \cdot \mu(H_{or}) \tag{15}$$

where constant $c_1 = (d\lambda / dH)_{\max}$. Coefficient $C_1$ is a constant, mainly dependent on the material and the fields at the excitation regions. Under these conditions $\mu(H_{or})$ is proportional to $V_o$.

In case that $H_e, H_{or}$ are constant and $H_{oe}$ changes, $V_o$ becomes:

$$V_o = -A \cdot a \cdot c \cdot H_e \cdot \mu(H_{or}) \cdot \frac{d\lambda}{dH} = C_2 \cdot \frac{d\lambda}{dH} \quad (16)$$

where $C_2$ is a constant, mainly dependent on the material and the excitation field and biasing field at the excitation and receiving regions respectively. Under these conditions $\frac{d\lambda}{dH}$ is proportional to $V_o$. When $H_{oe}, H_{or}$ are constant and $H_e$ changes, $V_o$ becomes:

$$V_o = -A \cdot a \cdot c \cdot H_e \cdot \mu(H_{or}) \cdot \frac{d\lambda}{dH} = C_3 \cdot H_e \cdot \frac{d\lambda}{dH} \quad (17)$$

Thus $\frac{V_o}{H_e} = C_3 \cdot \frac{d\lambda}{dH}$, where $C_3$ is a constant, mainly dependent on the material and the biasing fields at the excitation and receiving regions.

Apart from being useful in MDL behaviour description, this approach can also lead towards the use of this MDL arrangement for the experimental determination of the M-H and λ-H loops of magnetostrictive ribbons and wires as well as their corresponding uniformity functions. All the above mentioned equations used for the coil-coil MDL arrangement can also be used for the case of the next presented arrangement concerning conductors perpendicular to MDLs.

## 4. The MDL modeling used for the determination of magnetic properties

Following the theory developed in the previous chapter, the voltage output $V_o(t)$ at the search coil is given by equation 11:

$$V_o(t) = -A \cdot a \cdot \mu(H_{or}) \cdot \frac{d\lambda\left(H_{oe} + H_e(t)\right)}{dt} = \\ = -A \cdot a \cdot \mu(H_{or}) \cdot \frac{d\lambda}{dH} \frac{d\left(H_{oe} + H_e(t)\right)}{dt} \quad (18)$$

It will be hereinafter shown how this procedure can result in the experimental determination of the M-H and λ-H loops of magnetostrictive ribbons and wires as well as their corresponding uniformity functions [75].

*M-H loop*

Keeping the excitation and biasing fields at the excitation region $H_e$ and $H_{oe}$ respectively constant, while the biasing field $H_{or}$ at the receiving region changes, the peak amplitude of the MDL pulsed voltage output $V_o$ is given by equation 18 corresponding to the first derivative of $M(H_{or})$. Normalizing $V_o$ as well as its integral function and calibrating the MDL set-up using a standard Ni magnetostrictive wire of known M-H loop, the μ-H and M-H loops at the region of the receiving coil of the MDL can be determined. Since the applied biasing field is dc, the method determines the dc μ-H and M-H loops. As the sample is vibrated by the propagating elastic pulse, the method is an alternative vibrating sample magnetometer (VSM) technique, so it can be named MDL-VSM technique. A number of magnetostrictive ribbons and wires have been tested according to this method. In this report, indicative data of amorphous positive magnetostrictive ribbons and wires of the rather typical $Fe_{78}Si_7B_{15}$ composition are presented. Fig. 10a and 10b illustrate the dependence of the normalized MDL voltage output, which is equal to the magnetic permeability μ, as well as the magnetization M loops on the biasing field H, concerning an amorphous $Fe_{78}Si_7B_{15}$ magnetostrictive ribbon, after stress-current annealing under 400 MPa and 0.5 Å for 10 minutes. Fig. 11a and 11b illustrate the same response for the case of amorphous $Fe_{78}Si_7B_{15}$ ribbon after thermal annealing in 450 °C and Ar atmosphere for 1 h and consequent slow rate cooling. The observed hysteresis may be attributed to the partial crystallization of the ribbon. Such a technique can be used for studying various hysteretic properties of magnetostrictive materials.

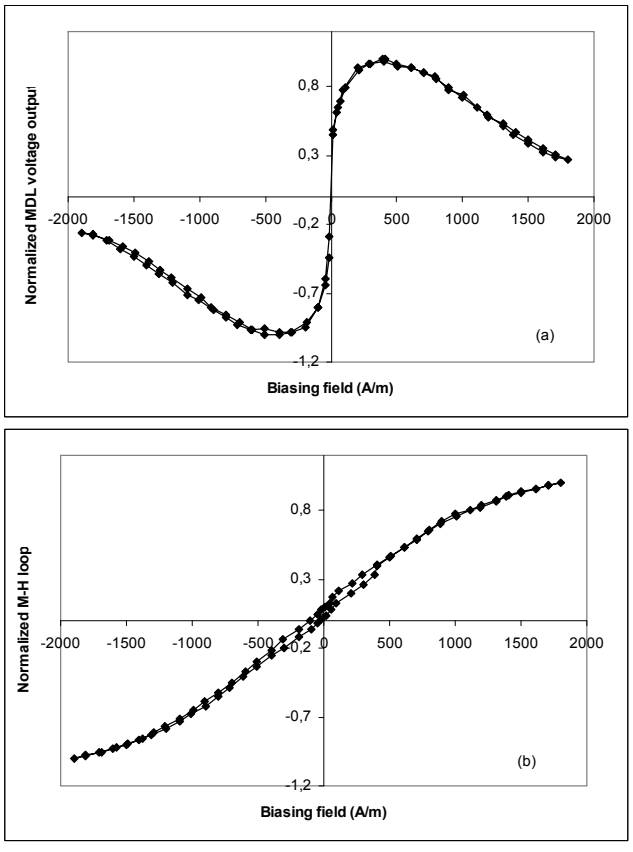


*Fig. 10. Permeability (a) and magnetization loops (b) concerning $Fe_{78}Si_7B_{15}$ amorphous wire after stress-current annealing.*

As an example the sharp and bistable behaviour of as-cast amorphous magnetostrictive $Fe_{78}Si_7B_{15}$ wires, corresponding to the Large Barkhausen jump, can be observed with this experiment, allowing the ability of observing the uniformity of the bistable behaviour along the length of the wire.

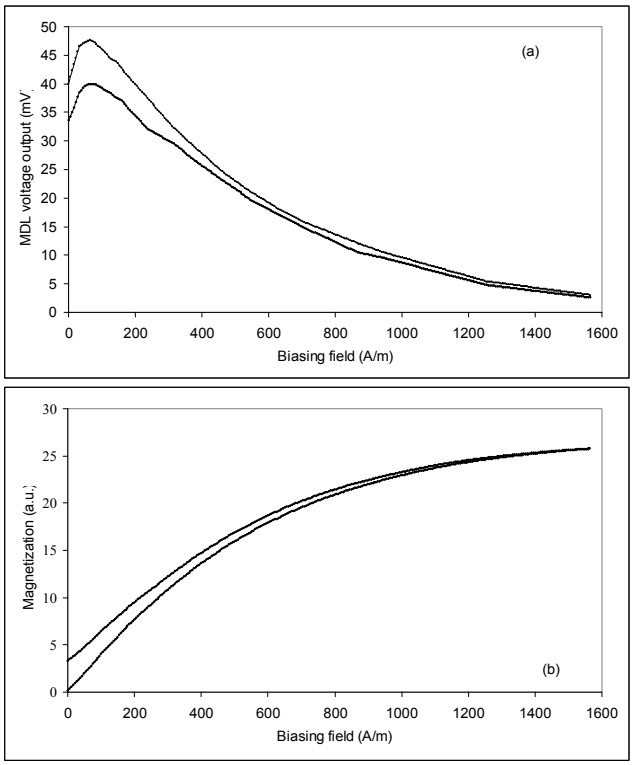


*Fig. 11. Permeability (a) and magnetization loops (b) concerning $Fe_{78}Si_7B_{15}$ amorphous ribbon after thermal annealing.*

<u>*λ-H loop*</u>

Keeping $H_e$ and $H_{or}$ constant, while the biasing field $H_{oe}$ changes, the peak amplitude of the MDL pulsed voltage output $V_o$ is given by equation 16, being proportional to $d\lambda(H_{oe})/dH$. Normalization process and calibration against a standard Ni magnetostrictive wire of known $\lambda$-$H$ loop results in the dc $\lambda$-$H$ function determination. Among various tested magnetostrictive materials, indicative results are presented concerning amorphous as-cast positive $Fe_{78}Si_7B_{15}$ magnetostrictive wires. Fig. 12a and 12b illustrate the normalized MDL response and the $\lambda$ dependence on $H_{oe}$ respectively.

Maintaining the basing fields $H_{oe}$ and $H_{or}$ steady and changing the excitation field $H_e$, the peak amplitude of $V_o/H_e$ is given by equation 17. Thus, the integral of $V_o/H_e$ on $H_e$ is proportional to the magnetostriction $\lambda$. Normalization and calibration against a standard Ni magnetostrictive wire of known $\lambda$-$H$ loop results in the $\lambda$-$H$ loop determination. Fig. 13a and 13b demonstrate indicatively the normalized MDL response and its integral corresponding to the λ-H function for the case of as-cast amorphous $Fe_{78}Si_7B_{15}$ wires.

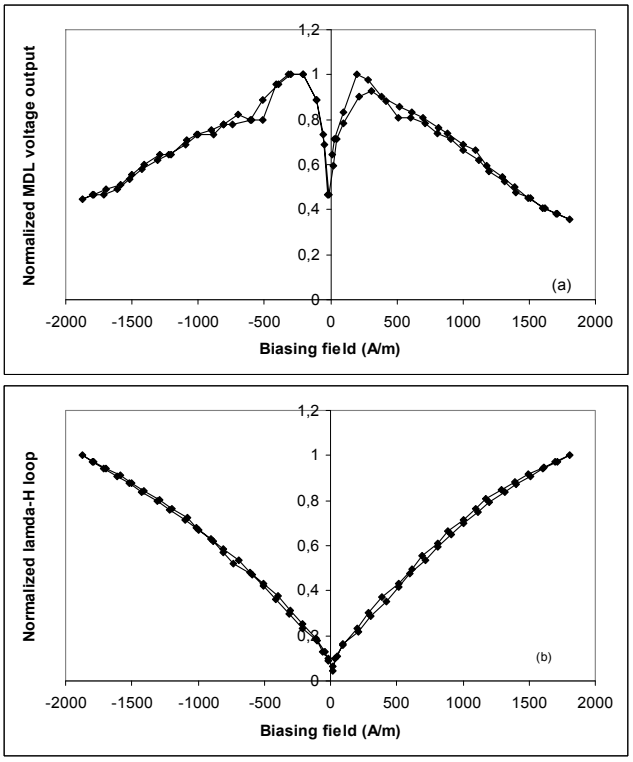


*Fig. 12. Normalized MDL response on biasing field at the excitation point (a) and integration of the MDL voltage output corresponding to the dc λ-H loop (b).*

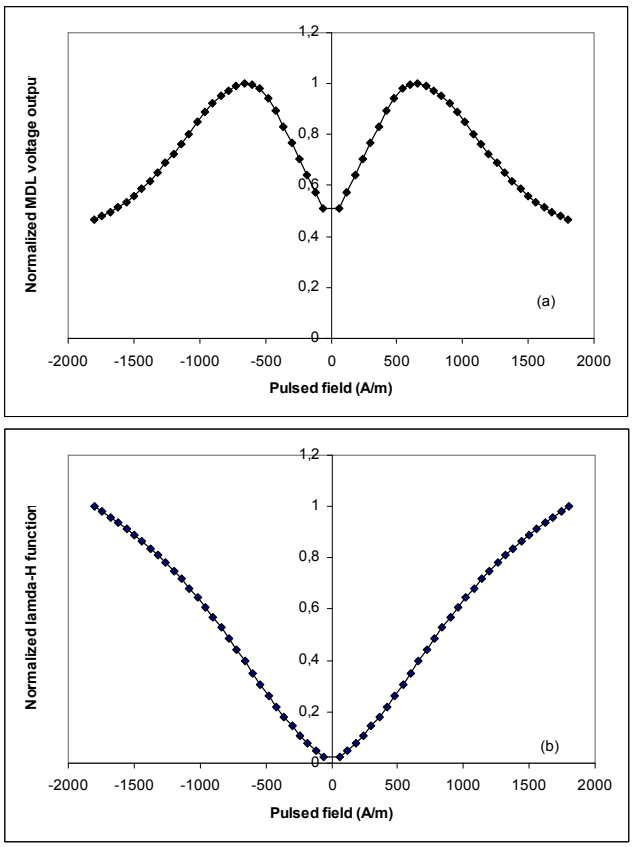


*Fig. 13. Normalized $V_o/H_e$ MDL response on the pulsed field (a) and integration of $V_o/H_e$ corresponding to the ac λ-H loop (b).*

*On the M(H) and λ(H) results*

The main advantage of the MDL-VSM technique with respect to the VSM technique is the by-design ability of non-destructive magnetic testing. Normally, in a classic VSM, the sample has to be cut in small pieces in order to be accommodated inside the VSM holder. Another significant advantage is the ability of measuring permeability, magnetization and flux density uniformity of the under test specimen, by moving the position of the receiving coil and the surrounding biasing coil.

Using this technique it is also possible to measure the M-H loop of magnetostrictive elements, not having the shape of acoustic waveguide by gluing them on a glass substrate. Thus the elastic pulse generated either by magnetostrictive or piezoelectric means, is coupled to the under test magnetostrictive specimen via the glass substrate and therefore, the dependence of μ and M may also be determined. This method can be also applied for the stress dependence determination of the M-H and λ-H loop.

Controlling the temperature of the set-up, one can determine the dependence of the μ-H, M-H and λ-H loops on temperature. Accordingly, changing the biasing field with a given frequency, always less than the frequency corresponding to the pulsed current excitation period, which is of the order of 1 ms thus corresponding to 1 kHz maximum limit of biasing field frequency, the dependence of μ-H, M-H and λ-H loops on frequency may also be determined. Temporal dependence tests of μ-H, M-H and λ-H loops may also be performed. All above mentioned applications may improve the implementation of magnetism and magnetic effects in engineering applications [76-79].

## 5. Conclusions

The generation, propagation and detection of an elastic pulse in the simplest MDL arrangements have been investigated. Such a study has resulted in understanding the mechanisms and parameters of elastic pulse generation and detection, namely being the excitation and biasing fields as well as the mechanical action on the MDL. Understanding these mechanisms and parameters allowed for the conceiving and development of new methods for determining the magnetic properties of magnetostrictive ribbons and wires.

## References

[1] E. O. Doebelin, Measurement Systems: applications and design, fourth edition, McCraw-Hill, 1990.
[2] E. E. Herceg, Handbook of measurement and control, rev. ed., Schaevitz Engineering, Pennsauken, N. J. 1976.
[3] R. Boll, Soft magnetic materials, Vacuumschmelze handbook, Heyden & Son, 1977.
[4] Magnetic Sensors and Magnetometers, P. Ripka (ed), Facem Meas. Sci. Technol., 13, 2002.
[5] J. M. Daughton, GMR applications, Journal of Magnetism and Magnetic Materials, **192**, 334 (1999).
[6] K. Mohri, K. Bushida, M. Noda, H. Yoshida, L. V. Panina, T. Uchiyama, Magneto-impedance element, IEEE Transactions on Magnetics **31**, 2455 (1995).
[7] E. du Tremolet de Lacheisserie, Magnetostriction: Theory and Applications of Magnetoelasticity, CRC Press, Boca Raton, FL, 1994
[8] J. D. Jackson, Electricity and Magnetism, Wiley, NY, 1965.
[9] D. Jiles, Introduction to the electronic properties of materials, Chapman & Hall, 1993.
[10] D. Jiles, Introduction to magnetism and magnetic materials, Chapman & Hall, 1991.
[11] R. C. O'Handley, Modern magnetic materials, Wiley, 1999.
[12] A. P. Thomas, M. R. J. Gibbs, J. H. Vincent, S. J. Ritchie, IEEE Transactions on Magnetics **27**, 5247 (1991).
[13] J. P. Hayes, L. A. Stone, H. V. Snelling, A. G. Jenner, R. D. Greenough, IEEE Transactions on Magnetics **33**, 3613 (1997).
[14] H. Chiriac, T. A. Ovari, J. Optoelectron. Adv. Mater. **4**, 367 (2002).
[15] A. Biekowski, Magnetoelastic Villari effect in Mn-Zn ferrites, Journal of Magnetism and Magnetic Materials, **215-216**, 231 (2000).
[16] A. Aharoni, Introduction to the theory of Ferromagnetism, Clarendon Press, Oxford, 1996.
[17] M. Onoe, J. Acoust. Soc. Am. **34**, 1247 (1962).
[18] I. Astefanoaei, H. Chiriac, A. Stancu, J. Optoelectron. Adv. Mater., **10**, 260 (2008).
[19] M. Mizutani, H. Katoh, L. V. Panina, K. Mohri, F. B. Humphrey, IEEE Transactions on Magnetics **29**, 3174 (1993).
[20] K. Kawashima, T. Kohzawa, H. Yoshida, K. Mohri, IEEE Transactions on Magnetics **29**, 3168 (1993).
[21] L. V. Panina, K. Mohri, Journal of Magnetism and Magnetic Materials, **157-158**, 137 (1996).
[22] A. Mitra, M. Vazquez, A. Hernando, C. Gomez-Polo, Field Flash Annealing of Co-Rich Amorphous Alloy, IEEE Transactions on Magnetics **26**, 1415 (1990).
[23] S. Chikazumi, Physics of Magnetism, John Wiley & Sons, 1964
[24] Y. H. Chen, D. C. Jiles, IEEE Transactions on Magnetics **37**, 3069 (2001).
[25] T. B. Thompson, J. A. M. Lyon, Analysis and application of magnetostrictive delay lines, Tranactions IRE PGUE-4, 8, 1956.
[26] K. G. Van den Berg, A multiple wire magnetostrictive delay line for improved signal and reduced reflections, J. Phys. E: Sci. Instrum. **15**, 325 (1982).
[27] M. Inoue, N. Fujita, T. Fujii, IEEE Transactions on Magnetics **20**, 1406 (1984).
[28] H. Epstein, O. B. Strum, Transactions IRE PGUE-5, 1, 1957.
[29] K. Kakuno, S. Masuda, T. Yamada, J. de Physique, C8, p. 2037, 1988.
[30] M. Inoue, Y. Tsuboi, A. Makita, N. Fujita, T. Miyama, T. Fujii, Japanese Journal of Applied Physics **25**, 157 (1986).
[31] P. T. Squire, M. R. J. Gibbs, Journal of Applied Physics **64**, 5408 (1988).

[32] M. G. Scott, A. Kursomovic, Metal. Sci. **15**, 583 (1981).
[33] K. Kakuno, S. Masuda, T. Yamada, H. Mochida, IEEE Transactions on Magnetics **23**, 2554 (1987).
[34] L. Lanotte. Z. Kaczkowski, L. Maritato, Europhys. Lett., **8**, 717 (1992).
[35] L. Lanotte, C. Luponio, A. Annunziata, Journal of Magnetism and Magnetic Materials, **80**, 153 (1989).
[36] N. Tsuya, K.I. Arai, T. Oksaka, IEEE Transactions on Magnetics, **14**, 946 (1978).
[37] M. Inoue, Study on propagation properties of magnetoelastic waves in Fe-based highly magnetostrictive amorphous materials and their applications, Doctoral Thesis, Toyohashi University of Technology, 1989
[38] R. D. James, Proceedings of the 5th Conference on Magnetic Materials Measurements and Modeling, Iowa State University, Ames, USA, 2002
[39] E. Quandt, Journal of Alloys and Compounds, **258**, 126 (1997).
[40] E. T. M. Lacey, D. G. Lord, P. J. Grundy, IEEE Transactions on Magnetics, **24**, 1713 (1988).
[41] M. Pasquale, A. Infortuna, L. Martino, C. Sasso, C. Beatrice, S. H. Lim, Journal of Magnetism and Magnetic Materials, **215-216**, 769 (2000).
[42] L. Kraus, F. Fendrych, P. Svec, J. Bydzovky, M. Kollar, J. Optoelectron. Adv. Mater., **4**, 237 (2002).
[43] S. Roth, H. Grahl, J. Degmova, N. Schlorke-de Boer, M. Stoica, J. M. Borrego, A. Conde, N. M. Mitrovic, J. Eckert, J. Optoelectron. Adv. Mater. **4**, 199 (2002).
[44] H. Gavrila, V. Ionita, J. Optoelectron. Adv. Mater. **4**, 173 (2002).
[45] H. Chiriac, M. Tibu, V. Dobrea, I. Murgulescu, J. Optoelectron. Adv. Mater., **6**, 647 (2004).
[46] A. F. Cobeño, A. P. Zhukov, E. Pina, J. M. Blanco, J. Gonzalez, J. M. Barandiaran, Journal of Magnetism and Magnetic Materials, **215-216**, 743 (2000).
[47] K. Imamura, S. Kwang-Ho, K. Ishiyama, M. Inoue, K. I. Arai, Anisotropy control of magnetostrictive film patterns, IEEE Transactions on Magnetics **37**, 2025 (2001).
[48] A. G. Jenner, J. P. Hayes, L. A. Stone, H. V. Snelling, R. D. Greenough, Applied Surface Science, **138-139**, 408 (1999).
[49] H. Chiriac, M. Pletea, E. Hristoforou, Sensors and Actuators A: Physical, **68**, 414 (1998).
[50] G. Herzer, IEEE Transactions on Magnetics **26**, 1397 (1990).
[51] P. Marín, M. López, P. Agudo, M. Vázquez, A. Hernando, Sensors and Actuators A: Physical **91**, 218 (2001).
[52] L. Lanotte, G. Ausanio, V. Iannotti, C. Luponio, Proceedings of the 4th European Magnetic Sensor and Actuator Conference, Athens, Greece, 2002
[53] J. L. Costa, Y. Makino, K. V. Rao, IEEE Transactions on Magnetics **26**, 1792 (1990).
[54] A. P. Thomas, M. R. J. Gibbs, P. T. Squire, IEEE Transactions on Magnetics, **26**, 1403 (1990).
[55] J. Gonzalez, J. M. Blanco, J. M. Barandiaran, M. Vazquez, A. Hernando, G. Rivero, D. Niarchos, IEEE Transactions on Magnetics **26**, 1798 (1990).
[56] L. Kraus, J. Phys. E: Sci. Instrum. **22**, 943 (1989).
[57] G. Vlasak, P. Duhaj, H. Patrasova, P. Svec, J. Phys. E: Sci. Instrum., **16**, 1203 (1983).
[58] Y. D. Shin, Y. H. Lee, J. R. Rhee, IEEE Transactions on Magnetics **29**, 3025 (1993).
[59] P. T. Squire, Meas. Sci. Technol. **5**, 67 (1994).
[60] M. Angelakeris, P. Poulopoulos, O. Valassiades, N. K. Flevaris, D. Niarchos, A. Nassiopoulou, Sensors and Actuators A: Physical, **91**, 180 (2001).
[61] M. Vazquez, K. L. Garcia, A. Zhukov, R. Varga, P. Vojtanik, J. Optoelectron. Adv. Mater. **6**, 581 (2004).
[62] V. Raposo, D. Garcia, O. Montero, A. G. Flores, J. I. Iniguez. J. Optoelectron. Adv. Mater. **6**, 575 (2004).
[63] L. P. Shen, T. Uchiyama, K. Mohri, E. Kita, K. Bushida, IEEE Transactions on Magnetics **33**, 3355 (1997).
[64] P. P. Freitas, F. Silva, N. J. Oliveira, L. V. Melo, L. Costa, N. Almeida, Sensors and Actuators A: Physical, **81**, 2 (2000).
[65] S. D. Kim, O. M. J. van't Erve, R. Jansen, P. S. Anil Kumar, R. Vlutters, J. C. Lodder, Sensors and Actuators A: Physical **91**, 166 (2001).
[66] K. Attenborough, H. Boeve, J. de Boeck, G. Borghs, J-P. Celis, Sensors and Actuators A: Physical **81**, 9 (2000).
[67] D. Kechrakos, K. N. Trohidou, Physica B: Condensed Matter, **318**, 360 (2002).
[68] K. Diaz de Lezana, A. García-Arribas, J. M. Barandiarán, J. Gutiérrez, Sensors and Actuators A: Physical, **91**, 226 (2001).
[69] O. V. Nielsen, P. Brauer, F. Primdahl, J. L. Jørgensen, C. Boe, T. Risbo, M. Deyerler, S. Bauereisen, Sensors and Actuators A: Physical **59**, 168 (1997).
[70] H. Chiriac, E. Hristoforou, M. Neagu, M. Pieptanariu, F. G. Castano, J. Appl. Phys. **87**(9), 5344 (2000).
[71] M. Inoue, N. Fujita, Journal of Applied Physics **73**, 6159 (1993).
[72] E. Hristoforou, Review Article, Meas. Sci. & Technol., **14**, R15 (2003).
[73] H. Hauser, E. Hristoforou, A. Ktena, MMM 2002, Tampa, Florida, USA, 2002
[74] H. Hauser, Proceedings of the 4th European Magnetic Sensor and Actuator Conference, Athens, Greece, 2002
[75] E. Hristoforou, P. Dimitropoulos, Journal of Magnetism and Magnetic Materials **304**, 164 (2006).
[76] E. Hristoforou, J. Optoelectron. Adv. Mater. **4**, 245 (2002).
[77] E. Koutroulis, A. G. Kladas, A. G. Mamalis, International Journal of Applied Electromagnetics and Mechanics, **13**, 285 (2002).
[78] A. G. Mamalis, D. E. Manolakos, A. G. Kladas, A. K. Koumoutsos, Applied Mechanics Reviews **57**, 299 (2004).
[79] S. Mohorianu, M. Lozovan, C. Baciu, J. Optoelectron. Adv. Mater. **9**, 1499 (2007).

*Corresponding author: eh@metal.ntua.gr